Article

TSP50 deficiency in neural stem cells aggravates colitis in mice by altering intestinal microbiome

Check for updates

Xiaoli Li[1,2], Rong Jin[2,3], Zhaoxia Wang[4], Chunxue Niu[1], Zhenbo Song[2], Xiaoling Liu[1], Jian Huang[1], Huan Zhang[4], Xia Qian[4], Feng Gao[2], Shuyue Wang[1], Chunlei Yu[3], Luguo Sun[1], Yanxin Huang[2], Lihua Zheng[2], Guannan Wang[2], Ying Sun[2], Xiaoguang Yang[3,5] ✉, Yongli Bao[2,5] ✉ & Jiawei Li[1,5] ✉

Inflammatory bowel disease (IBD) is a complex disease characterized by persistent chronic inflammation of the gastrointestinal tract and periodic episodes. Despite the increasing number of related studies, the detailed pathogenesis of IBD has not been elucidated. In recent years, host-microbiota interactions in the pathogenesis of IBD have received extensive attention. Testes-specific protease 50 (TSP50) is a potential risk gene for IBD, but whether it can affect the susceptibility of colitis by regulating the gut microbiome is still unclear. Here, we showed that TSP50 deficiency in neural stem cells (NSCs) aggravated colitis in mice by altering intestinal microbiome. Mechanistically, TSP50 maintained the level of neurotransmitter acetylcholine (ACh) by degrading acetylcholinesterase (AChE), thereby maintaining intestinal mucosa and intestinal microecological homeostasis and reducing the susceptibility to colitis. These findings provide a new perspective on the interaction between host and commensal microbiota, which may be beneficial for developing potential therapeutic strategies for IBD.

Inflammatory bowel disease (IBD), encompassing Crohn's disease (CD) and Ulcerative colitis (UC), is among the most prevalent gastrointestinal diseases worldwide[1,2]. Due to the complexity of the pathogenesis of IBD, effective treatments are currently lacking[3,4]. Therefore, it is urgent to elucidate the precise pathogenesis of IBD and develop novel therapeutic strategies.

The gut microbiome has long been thought to play a key role in human health and disease[5]. Under normal physiological conditions, the gut microbiota protects intestinal mucosal integrity as the first line of defense against pathogenic microorganisms and produces short-chain fatty acids (SCFAs), which have anti-inflammatory effects[6,7]. Dysbiosis of gut microbiota, particularly a reduction in the abundance and diversity of specific genera, is thought to be a trigger in the development of IBD[8]. It has been shown that the enteric nervous system (ENS) plays an important role in shaping intestinal microecology[9]. In addition, the autonomic nervous system (ANS) dysregulation can reduce intestinal mucosal barrier integrity and lead to microbial dysregulation[10]. Accumulating evidence has shown that

neurotransmitters play an important role in promoting microbial adaptability[11–13]. However, as a major neurotransmitter in the central and peripheral nervous systems, the role of acetylcholine (ACh) in regulating intestinal microecology is still unclear.

Numerous studies have shown that gene-microbiota interactions contribute to the pathogenesis of IBD, such as nucleotide binding oligomerization domain 2 (NOD2) or autophagyrelated16-like1 (ATG16L1)[14–16]. Testes-specific protease 50 (TSP50) is a serine hydrolase expressed in various tissues, including the brain and gut[17]. It is involved in the regulation of various physiological processes, including cell proliferation[18], spermatogenesis[19], embryonic development[20], neurodevelopment[21], and intestinal homeostasis. Previous studies in our laboratory have shown that TSP50 in intestinal stem cells protects mice against DSS-induced colitis by regulating TGF-β signaling pathway[22]. Although TSP50 plays a decisive role in maintaining intestinal mucosal barrier, its roles in shaping the gut bacterial ecology have not been investigated in depth.

[1]National Engineering Laboratory for Druggable Gene and Protein Screening, Northeast Normal University, Changchun, China. [2]International Joint Research Center of Stem Cell Bank, Ministry of Science and Technology, Northeast Normal University, Changchun, China. [3]The Key Laboratory of Molecular Epigenetics of Ministry of Education, Northeast Normal University, Changchun, Jilin, China. [4]Department of Gastroenterology, Shenzhen Children's Hospital, Shenzhen, Guangdong, China. [5]These authors contributed equally: Xiaoguang Yang, Yongli Bao, Jiawei Li. ✉e-mail: yangxg168@nenu.edu.cn; baoyl800@nenu.edu.cn; lijw447@nenu.edu.cn

In this study, we found that TSP50 deficiency in neural stem cells (NSCs) increased susceptibility of mice to dextran sulfate sodium (DSS)-induced colitis, which was dependent on the gut microbiota. Furthermore, our findings revealed that TSP50 deficiency in NSCs resulted in ANS disorders and decreased ACh levels. Mechanistically, TSP50 deficiency in NSCs reduced ACh levels by reducing acetylcholinesterase (AChE) degradation, leading to altered gut homeostasis. ACh supplementation restored the intestinal mucosal barrier damage and microbiome alterations induced by NSCs TSP50 deficiency, and decreased susceptibility to colitis. Collectively, our results highlight the critical role of TSP50 in NSCs in maintaining intestinal homeostasis and protecting mice from colitis, particularly through its regulation of gut microbiome. These findings provide a new perspective on gene-nervous system-gut microbiota trilateral relationship, which may be beneficial for the design of novel therapeutic approaches to alleviate IBD.

Results

TSP50 deficiency in NSCs increases susceptibility of mice to DSS-induced colitis

It has been noted that TSP50 influences neurodevelopment[21], and TSP50 deficiency in intestinal stem cells can aggravate DSS-induced colitis[22]. Given the important role of the nervous system in regulating gastrointestinal tract function[23,24], we hypothesized that TSP50 may influence IBD susceptibility through its action on the nervous system. To explore this hypothesis, we engineered NSCs-specific knockout TSP50 mice-*TSP50^{fl/fl}Nestin^{Cre}* mice. Immunofluorescence staining of TSP50 in brain tissue sections from embryonic day 16.5 (E16.5) demonstrated that TSP50 was absent in brain NSCs of *TSP50^{fl/fl}Nestin^{Cre}* mice (Supplementary Fig. 1a), which was confirmed by RT-qPCR and western blotting conducted on isolated embryonic brain tissues (Supplementary Fig. 1b, c). Similar results were observed in the intestinal tissues of *TSP50^{fl/fl}Nestin^{Cre}* mice on E16.5 (Supplementary Fig. 1d–f) To determine whether there is a causal relationship between TSP50 expression in NSCs and IBD susceptibility, we induced experimental colitis in both control and *TSP50^{fl/fl}Nestin^{Cre}* mice by oral administration of 2.5% DSS for seven consecutive days (Fig. 1a). Compared with control mice, *TSP50^{fl/fl}Nestin^{Cre}* mice showed increased susceptibility to colitis, as demonstrated by greater weight loss, higher DAI scores, lower survival rates, and shorter colon lengths (Fig. 1b–e). HE staining of colon tissue sections showed aggravated pathological changes in *TSP50^{fl/fl}Nestin^{Cre}* mice, including complete destruction of crypt structure and abnormal infiltration of inflammatory cells, which resulted in higher histopathological scores (Fig. 1f). In addition, the *TSP50^{fl/fl}Nestin^{Cre}* mice exhibited higher levels of proinflammatory factors, including tumor necrosis factor-α (TNF-α) and interleukin- 6 (IL-6), in their serum, indicating a greater degree of systemic inflammation (Fig. 1g, h). Together, these data show that TSP50 deficiency in NSCs enhances the susceptibility of mice to DSS-induced colitis.

TSP50 deficiency in NSCs leads to intestinal mucosal barrier damage

Previous studies have clearly established the critical role of the intestinal mucosal barrier in the pathogenesis of colitis[25]. To further explore the specific mechanism by which TSP50 deficiency in NSCs leads to increased susceptibility to colitis, we examined the effect of TSP50 deficiency in NSCs on intestinal mucosal barrier under normal conditions. Intestinal histomorphology examination showed that colon length and colon tissue morphology were not altered in *TSP50^{fl/fl}Nestin^{Cre}* mice compared with control mice (Supplementary Fig. 2a, b); the intestinal mucosal mechanical barrier was also not altered (Supplementary Fig. 2c, d). However, compared with control mice, *TSP50^{fl/fl}Nestin^{Cre}* mice presented a significant reduction in the number of goblet cells and decreased levels of MUC2 protein (Fig. 2a, b and Supplementary Fig. 2e), whereas no differences were observed in the mRNA levels of stemness-associated proteins (LGR5, BMI, and MSI) (Supplementary Fig. 2f). Next, we evaluated the functions of TSP50 in NSCs in vitro conditions using small intestinal organoids from control and *TSP50^{fl/fl}Nestin^{Cre}* mice. Compared with organoids from control mice, those obtained from *TSP50^{fl/fl}Nestin^{Cre}* mice exhibited a similar formation rate, but

the number of buddings was significantly reduced (Fig. 2c, d). Consistent with the in vivo data, the number of goblet cells and the MUC2 protein levels were significantly decreased in *TSP50^{fl/fl}Nestin^{Cre}* organoids compared to controls (Fig. 2e, f).

Decreased mucin secretion can lead to intestinal mucosal barrier damage and increased barrier permeability, thereby facilitating the occurrence of intestinal inflammation[26]. The results of bacterial translocation experiments showed that bacterial translocation occurred in intestinal mesentery of *TSP50^{fl/fl}Nestin^{Cre}* mice (Fig. 2g). Moreover, we observed that serum lipopolysaccharides (LPS) levels and colon proinflammatory cytokines TNF-α and IL-6 levels were significantly increased in *TSP50^{fl/fl}Nestin^{Cre}* mice, suggesting impaired intestinal mucosal barrier function and that direct contact between the gut microbiota and the intestinal epithelium triggered intestinal inflammation in *TSP50^{fl/fl}Nestin^{Cre}* mice (Fig. 2h–j).

TSP50 deficiency in NSCs changes intestinal microbiota and reduces SCFAs production

There is a close interaction between intestinal microbiota and intestinal mucosal barrier, and the change of intestinal mucosal barrier is likely to lead to the change of intestinal microbiota[27]. To determine whether the gut microbiota changed in *TSP50^{fl/fl}Nestin^{Cre}* mice, we collected fecal samples from control and *TSP50^{fl/fl}Nestin^{Cre}* mice for 16S rRNA sequencing. Principal coordinates analysis (PCoA) revealed major differences in the microbial composition between control and *TSP50^{fl/fl}Nestin^{Cre}* mice (Fig. 3a). Histograms of species composition at phylum and genus levels showed the same results as for PCoA (Fig. 3b, c). Species composition difference analysis at phylum level revealed that *TSP50^{fl/fl}Nestin^{Cre}* mice had a lower abundance of Verrucomicrobia and a higher abundance of Tenericutes and Deferribacteres (Fig. 3d). Species composition difference analysis at genus level further showed that *Akkermansia* genus was significantly reduced in *TSP50^{fl/fl}Nestin^{Cre}* mice compared to control mice, and it was the only differentially abundant genus among the TOP10 most abundant taxa (Fig. 3e). Heatmap analysis also revealed a significant reduction in *Akkermansia* genus in *TSP50^{fl/fl}Nestin^{Cre}* mice (Fig. 3f). In addition, LEfSe and LDA analysis identified *Akkermansia* and *Bacteroides* as the key bacterial taxa significantly enriched in the control and *TSP50^{fl/fl}Nestin^{Cre}* groups, respectively (Fig. 3g). These observations indicate that TSP50 deficiency in NSCs results in alterations in intestinal microbiota composition.

SCFAs are the main metabolites produced by intestinal microbiota, which can regulate immune function and delay the clinical progression of IBD[28]. Measurement of SCFAs concentrations in fecal samples revealed a significant decrease of acetic acid levels in *TSP50^{fl/fl}Nestin^{Cre}* mice compared with control mice (Fig. 3h). Taken together, these results demonstrate that TSP50 deficiency in NSCs changes the composition of intestinal microbiota and reduces SCFAs production.

Exacerbation of colitis in *TSP50^{fl/fl}Nestin^{Cre}* mice depends on the gut microbiota

To determine whether a microbiota-dependent mechanism contributes to deterioration of colitis, we treated control and *TSP50^{fl/fl}Nestin^{Cre}* mice with an antibiotic cocktail (ABX) for 4 weeks to consume their gut microbiota before DSS treatment (Supplementary Fig. 3a). Surprisingly, antibiotic treatment eliminated differences in the severity of colitis including body weight loss, DAI scores, survival rates, colon length, histological scores, and serum proinflammatory factors levels between control and *TSP50^{fl/fl}Nestin^{Cre}* mice (Supplementary Fig. 3b–h), suggesting that the gut microbiota may play a crucial role in worsening colitis in *TSP50^{fl/fl}Nestin^{Cre}* mice.

To further verify whether the deterioration of colitis caused by TSP50 deficiency in NSCs is due to gut microbiota dysbiosis, we cohoused control mice with *TSP50^{fl/fl}Nestin^{Cre}* mice for 4 weeks prior to DSS treatment (Supplementary Fig. 4a). Cohoused *TSP50^{fl/fl}Nestin^{Cre}* mice showed symptoms of colitis comparable to those observed in cohoused control mice and showed milder symptoms of colitis relative to non-cohoused *TSP50^{fl/fl}Nestin^{Cre}* mice (Supplementary Fig. 4b–h),
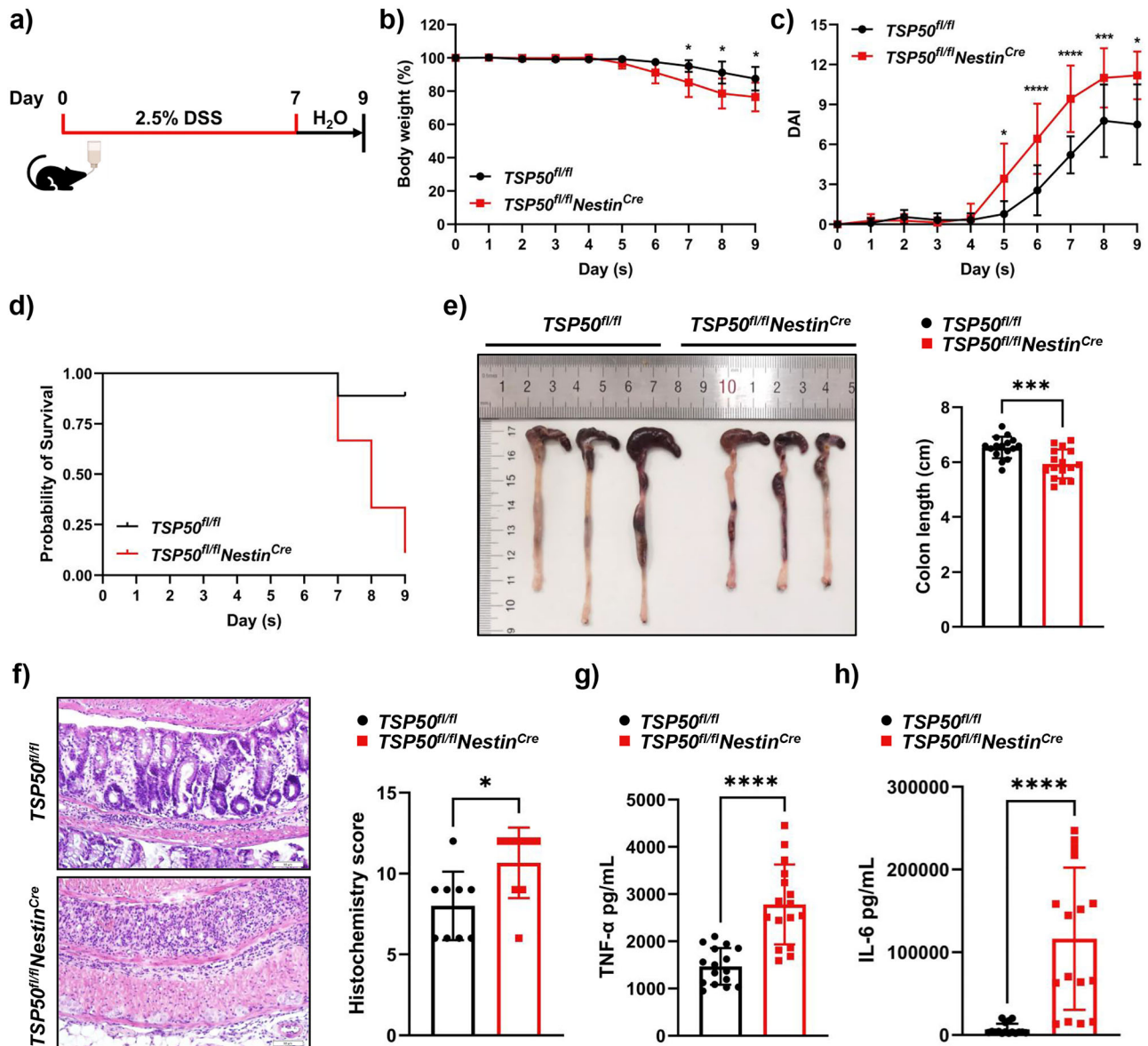
Fig. 1 | TSP50 deficiency in NSCs increases susceptibility of mice to DSS-induced colitis. a Experimental design of DSS-induced colitis. **b** Body weight loss after DSS treatment ($n = 16$). **c, d** The DAI scores and survival rates after DSS treatment ($n = 16$). **e** Colon lengths and quantification after DSS treatment ($n = 16$). **f** Representative HE staining and histopathological scores of colon tissues after DSS treatment ($n = 9$). Scale bar: 50 μm. **g** ELISA analysis of serum TNF-α levels after DSS treatment ($n = 16$). **h** ELISA analysis of serum IL-6 levels after DSS treatment ($n = 16$). Values were expressed as means ± SEM. Two-way ANOVA was used to analyze (**b, c**) unpaired two-tailed Student's *t* test was used to analyze (**e, f, g, h**). ns (no significance), * $P < 0.05$, ** $P < 0.01$, *** $P < 0.001$, **** $P < 0.0001$.

indicating gut microbiota contributes to the attenuated DSS-induced colitis phenotype in *TSP50^{fl/fl}Nestin^{Cre}* mice.

Given the disordered gut microbiota and reduced *Akkermansia* genus abundance in *TSP50^{fl/fl}Nestin^{Cre}* mice, we rescued the increased susceptibility to colitis in these mice with fecal microbiota transplantation (FMT) and *Akkermansia muciniphila* (AKK) replantation (Fig. 4a). As evidenced by body weight loss, DAI scores, survival rates, colon length, histological scores, and serum inflammatory factors levels, *TSP50^{fl/fl}Nestin^{Cre}* mice exhibited increased resistance to colitis after FMT and AKK supplementation (Fig. 4b–h), demonstrating that gut microbiota disturbance, especially the reduction of *Akkermansia* genus, may be a decisive factor in increased susceptibility to colitis in *TSP50^{fl/fl}Nestin^{Cre}* mice.

Furthermore, the SCFAs levels produced by fecal bacteria were comparable between control and *TSP50^{fl/fl}Nestin^{Cre}* mice after cohousing (Supplementary Fig. 5a). Notably, in *TSP50^{fl/fl}Nestin^{Cre}* mice treated with FMT and AKK replantation, the fecal bacterial SCFAs levels returned to normal

(Supplementary Fig. 5b). However, the differences in goblet cell numbers and MUC2 protein expression between control and *TSP50^{fl/fl}Nestin^{Cre}* mice were not altered after modulation of gut microbiota (Supplementary Fig. 5c–h). These data collectively suggest that alterations of intestinal microbiome may account for the colitis phenotype in *TSP50^{fl/fl}Nestin^{Cre}* mice, and that reduced mucin secretion is a direct result of genetic defects in TSP50.

TSP50 deficiency in NSCs results in ANS disorders and reduced ACh levels

To further explore the specific mechanism observed above, we examined the effect of TSP50 deficiency in NSCs on the central nervous system (CNS) under normal conditions. Nissl staining showed that there was no significant change in the morphological structure of the brain in *TSP50^{fl/fl}Nestin^{Cre}* mice (Supplementary Fig. 6a). To further examine the effect of TSP50 deficiency in NSCs on the CNS, we systematically examined inflammatory cytokine levels in four key CNS regions: the cortex,
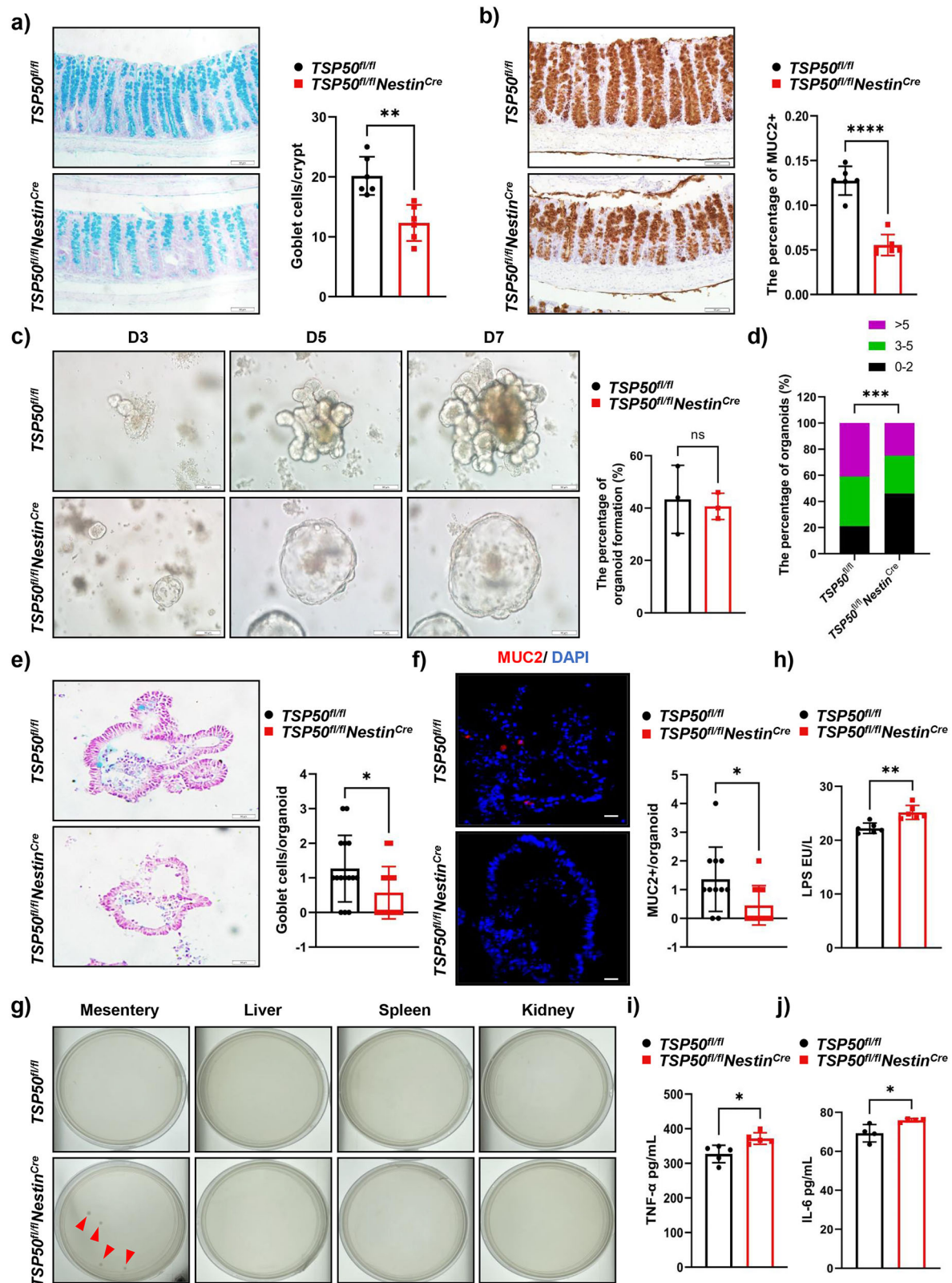
hippocampus, hypothalamus, and pituitary gland. The ELISA results showed that there were no statistically significant changes in inflammatory cytokines such as TNF-α and IL-6 in these regions of NSCs TSP50-deficient mice (Supplementary Fig. 6b–i). Additionally, serum analyses of hormones related to the hypothalamic-pituitary-adrenal (HPA) axis, such as adreno-corticotropic hormone (ACTH), corticotropin-releasing hormone (CRH)

and corticosterone (CORT), C-reactive protein (CRP), and systemic inflammatory cytokines TNF-α and IL-6 also showed no differences between the two groups (Supplementary Fig. 6j–o). Collectively, these results indicate that TSP50 deficiency in NSCs does not cause detectable structural disruption or CNS inflammation. However, heart rate variability analysis revealed that the vagus nerve was depressed, and the sympathetic

Fig. 2 | TSP50 deficiency in NSCs reduces goblet cell numbers and mucin secretion, increases mucosal permeability and intestinal inflammation. **a** Representative alcian blue staining of colon tissues and quantification under normal condition ($n = 6$). Scale bar: 50 μm. **b** Representative IHC staining of MUC2 expression in colon tissues and quantification under normal condition ($n = 6$). Scale bar: 50 μm. **c** Representative images and quantification of small intestinal organoid cultures on day 7 ($n = 3$, n represents the number of wells in which organoids were cultured). Scale bar: 50 μm. **d** Quantification of the proportion of organoids with different budding numbers on day 7 of the organoid culture ($n = 50$, n represents the number of organoids observed from the same well). **e** Representative alcian blue staining of small intestinal organoids and quantification ($n = 15$, n represents the number of intact organoids observed in organoid sections from the same well). Scale

bar: 20 μm. **f** Representative IF staining of MUC2 expression in small intestinal organoids and quantification ($n = 11$, n represents the number of intact organoids observed in organoid sections from the same well). Scale bar: 20 μm. **g** Bacterial translocation in mesentery, liver, spleen and kidney under normal condition. Red arrows point to colonies that have undergone displacement. **h** ELISA analysis of serum LPS levels under normal condition ($n = 6$). **i** ELISA analysis of colon TNF-α levels under normal condition ($n = 5$). **j** ELISA analysis of colon IL-6 levels under normal condition ($n = 4$). Values were expressed as means ± SEM. Unpaired two-tailed Student's t test was used to analyze (**a**, **b**, **c**, **e**, **f**, **h**, **i**, **j**), chi-square test was used to analyze (**d**). ns (no significance), * $P < 0.05$, ** $P < 0.01$, *** $P < 0.001$, **** $P < 0.0001$.

nervous systems (SNS) and parasympathetic nervous systems (PNS) were unbalanced in *TSP50^{fl/fl}Nestin^{Cre}* mice (Fig. 5a–d). To explore the cause of the ANS imbalance in *TSP50^{fl/fl}Nestin^{Cre}* mice, we performed untargeted metabolic sequencing on the brains of the mice. The results indicated that the relative content of the neurotransmitter ACh was significantly reduced in the hippocampal region of the brains of *TSP50^{fl/fl}Nestin^{Cre}* mice compared with control mice (Fig. 5e). The significant reduction in ACh levels in the brains of *TSP50^{fl/fl}Nestin^{Cre}* mice was further confirmed by ELISA (Fig. 5f). Given that neurotransmitters play important roles in both the brain and the gut, and that the ENS is present in the gut, colonic neurotransmitters were measured in control and *TSP50^{fl/fl}Nestin^{Cre}* mice. The results showed that compared with controls, colonic ACh was reduced in *TSP50^{fl/fl}Nestin^{Cre}* mice, whereas no significant differences were observed in the other neurotransmitters examined, indicating that TSP50 in NSCs most likely plays a regulatory role in intestinal homeostasis by regulating ACh levels (Fig. 5g).

ACh supplementation restores the intestinal mucosal barrier damage and microbiome alterations induced by NSCs TSP50 deficiency

To test whether decreased ACh levels contributed to the disruption of mucosal barrier in *TSP50^{fl/fl}Nestin^{Cre}* mice, we administered ACh via enema every other day to control and *TSP50^{fl/fl}Nestin^{Cre}* mice. The ELISA results indicated that ACh enema increased colonic ACh levels in mice and eliminated the difference in colonic ACh content between control and *TSP50^{fl/fl}Nestin^{Cre}* mice (Fig. 6a). Consistently, administration of an ACh supplementation abolished the differences in goblet cell numbers and MUC2 protein levels between control and *TSP50^{fl/fl}Nestin^{Cre}* mice (Supplementary Fig. 7a, b). Furthermore, when 100 μM ACh was added on the third day of organoid culture, the budding rate of organoids from *TSP50^{fl/fl}Nestin^{Cre}* mice increased, and the number of goblet cells and MUC2 expression also returned to normal (Supplementary Fig. 7c–f). In addition, ACh supplementation also abolished differences in intestinal mucosal permeability and intestinal inflammation between control and *TSP50^{fl/fl}Nestin^{Cre}* mice (Supplementary Fig. 7g–j).

To investigate whether ACh has a regulatory effect on microbiota, 16S rRNA sequencing was used to analyze the diversity and composition of fecal microbiota in control mice, *TSP50^{fl/fl}Nestin^{Cre}* mice, ACh-treated control mice and ACh-treated *TSP50^{fl/fl}Nestin^{Cre}* mice. Consistent with the previous results, PCoA showed a statistically significant difference in microbiota between control and *TSP50^{fl/fl}Nestin^{Cre}* mice. Additionally, PCoA showed a statistically significant difference in microbiota between *TSP50^{fl/fl}Nestin^{Cre}* mice and ACh-treated *TSP50^{fl/fl}Nestin^{Cre}* mice, whereas the gut microbiota of *TSP50^{fl/fl}Nestin^{Cre}* mice receiving ACh treatment was like that of control mice (Fig. 6b). Histograms of species composition at phylum and genus levels showed the same results as for PCoA (Fig. 6c, d). Analysis of species composition difference further revealed that the abundance of Verrucomicrobia phylum and *Akkermansia* genus were significantly increased in both control and *TSP50^{fl/fl}Nestin^{Cre}* mice after ACh treatment. In addition, ACh treatment significantly increased the abundance of *Ruminococcus* genus and decreased the abundance of *Mucispirillum* genus in control mice (Fig. 6e, f). The species composition heatmap and LEfSe analysis showed the same experimental results (Fig. 6g–i). Moreover, the levels of SCFAs in the

fecal microbiota of ACh-treated *TSP50^{fl/fl}Nestin^{Cre}* mice were also significantly increased (Fig. 6j). Collectively, these results suggested that intestinal mucosal barrier damage in *TSP50^{fl/fl}Nestin^{Cre}* mice is caused by reduced ACh levels, and ACh supplementation restores intestinal mucosal barrier damage and gut microbiome, especially of *Akkermansia* genus, in *TSP50^{fl/fl}Nestin^{Cre}* mice.

Furthermore, to further elucidate the causal relationship between ACh and gut microbiota, ACh levels in the colon of mice after ABX, cohabitation, FMT and AKK replantation were examined. The results showed that the levels of ACh in the colon of mice did not change significantly after the modulation of gut microbiota (Fig. 6k–m). Combined with the above results that ACh supplementation altered gut microbiota in mice, we believe that ACh has a positive regulatory relationship with gut microbiota.

ACh supplementation reduces colitis susceptibility in mice

To further explore the potential of ACh to ameliorate colitis in *TSP50^{fl/fl}Nestin^{Cre}* mice, DSS-induced colitis was administered to mice during ACh supplementation as shown in Supplementary Fig. 8a. As expected, ACh treatment attenuated the symptoms of DSS-induced colitis and eliminated differences in susceptibility to colitis between control and *TSP50^{fl/fl}Nestin^{Cre}* mice. This was evidenced by the normalization of percent weight loss, DAI scores, survival rates, colon length, histological scores, and serum proinflammatory cytokines levels (Supplementary Fig. 8b–h). In conclusion, these data strongly suggest that TSP50 may maintain intestinal homeostasis and reduce the susceptibility to colitis by regulating ACh levels.

TSP50 deficiency in NSCs reduces ACh levels by reducing AChE degradation

Previous studies have shown that AChE is a highly efficient hydrolase that catalyzes the hydrolysis of ACh[29]. To investigate whether the decreased ACh content in *TSP50^{fl/fl}Nestin^{Cre}* mice was associated with AChE, AChE expression levels in mouse brain and colon were examined. We found that *TSP50^{fl/fl}Nestin^{Cre}* mice had reduced AChE protein expression in both the brain and colon (Fig. 7a). To further explore the specific mechanism, we performed Co-IP experiments and discovered that TSP50 can bind AChE in both mouse brain and colon (Fig. 7b). The GST-pulldown assay further demonstrated that TSP50 can directly bind to AChE (Fig. 7c). To exclude the possibility that the decreased AChE content was due to reduced protein synthesis, the protein synthesis inhibitor CHX was used. 293T cells treated with 100 μg/mL CHX for 6 h showed a decrease in AChE levels; most importantly, the TSP50-overexpressing cells contained significantly and persistently lower AChE levels than the control cells (Fig. 7d), indicating that TSP50 expression significantly increased the rate of AChE degradation. To test whether TSP50 had a direct degradation effect on AChE, purified TSP50 protein and AChE protein were mixed and incubated in 20 mmol/L Tris-HCl (pH 7.6) at 37 °C for 1 h to restore the protease activity of TSP50, and then AChE protein levels were measured. As expected, the AChE protein levels were greatly reduced (Fig. 7e), suggesting that TSP50 acts as a protease that can directly interact with and hydrolyze AChE proteins. Previous studies have shown that the catalytic triplet structure of TSP50
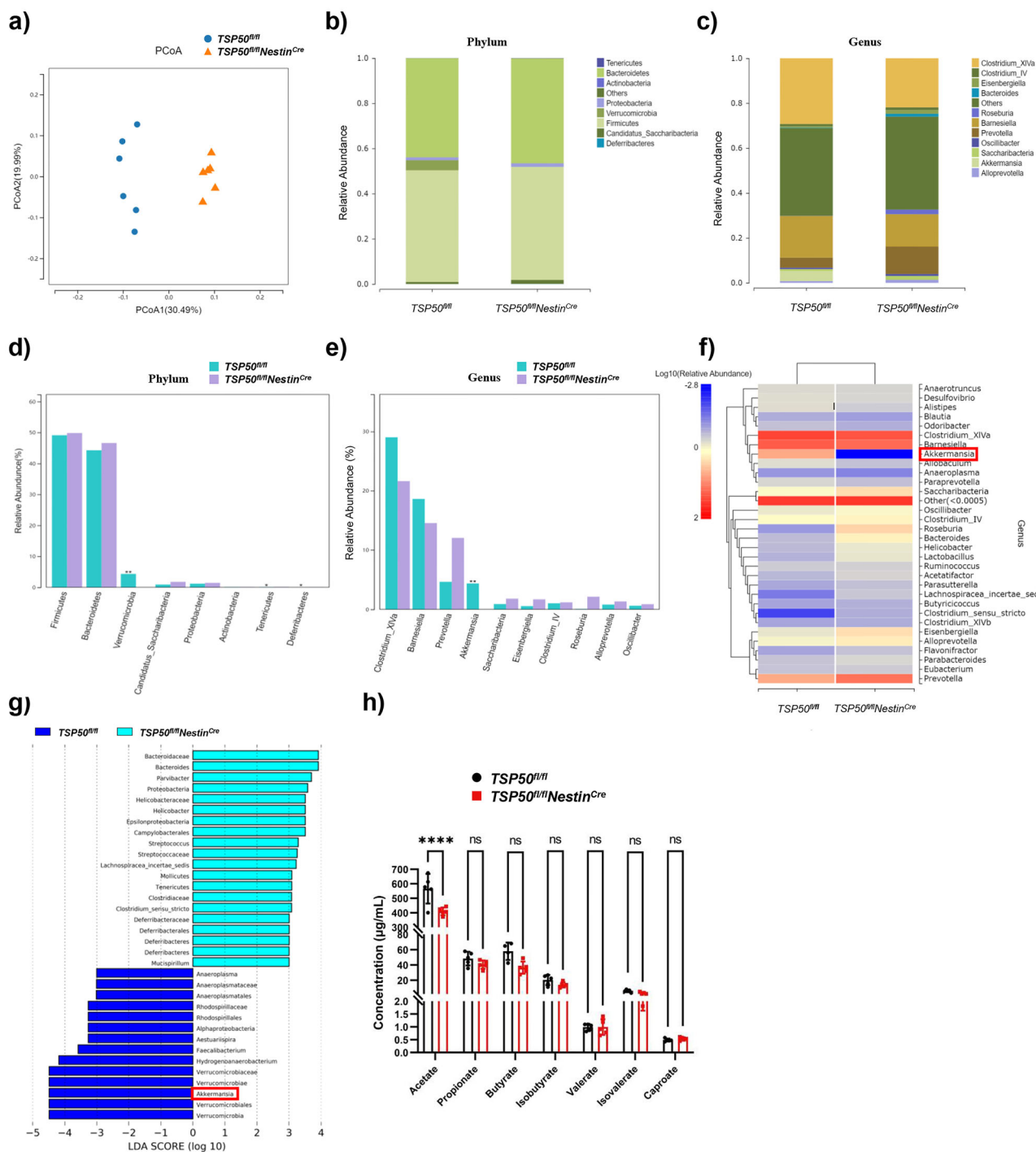
Fig. 3 | TSP50 deficiency in NSCs alters intestinal microbiota and reduces SCFAs production. a PCoA analysis of fecal microbiota using weighted UniFrac distances of beta diversity. **b** Histogram of phylum-level species composition. **c** Histogram of genus-level species composition. **d** Histogram of species difference comparison for the top 10 abundances at phylum-level ($n = 6$). **e** Histogram of species difference comparison for the top 10 abundances at genus-level ($n = 6$). **f** Heat map of the relative abundance of the dominant genus. **g** LEfSe analysis of differential microbiota. **h** GC-MS analysis of fecal SCFAs ($n = 5$). Values were expressed as means ± SEM. Mann-Whitney U-test was used to analyze (**d**, **e**), one-way ANOVA was used to analyze (**h**). ns (no significance), * $P < 0.05$, ** $P < 0.01$, *** $P < 0.001$, **** $P < 0.0001$.

is essential for its biological functions[18], so we established three point mutant constructs in the catalytic triad, named TSP50 T310A, TSP50 D206A and TSP50 H153A, respectively, to explore the key sites where TSP50 exerts its effect on AChE hydrolysis. The results revealed that AChE expression was not reduced only in TSP50 D206A-expressing cells (Fig. 7f), suggesting that aspartic acid at position 206 of TSP50 may play a key role in the hydrolysis of AChE.

TSP50 expression is negatively correlated with AChE expression in IBD patients

To investigate the relationship between TSP50 and AChE expression in IBD patients, we next assessed TSP50 and AChE protein expression in intestinal tissues from CD patients during the active and remission phases. All samples ($n = 19$) of CD patients were obtained from Shenzhen Children's Hospital. Immunohistochemical staining showed that TSP50 protein
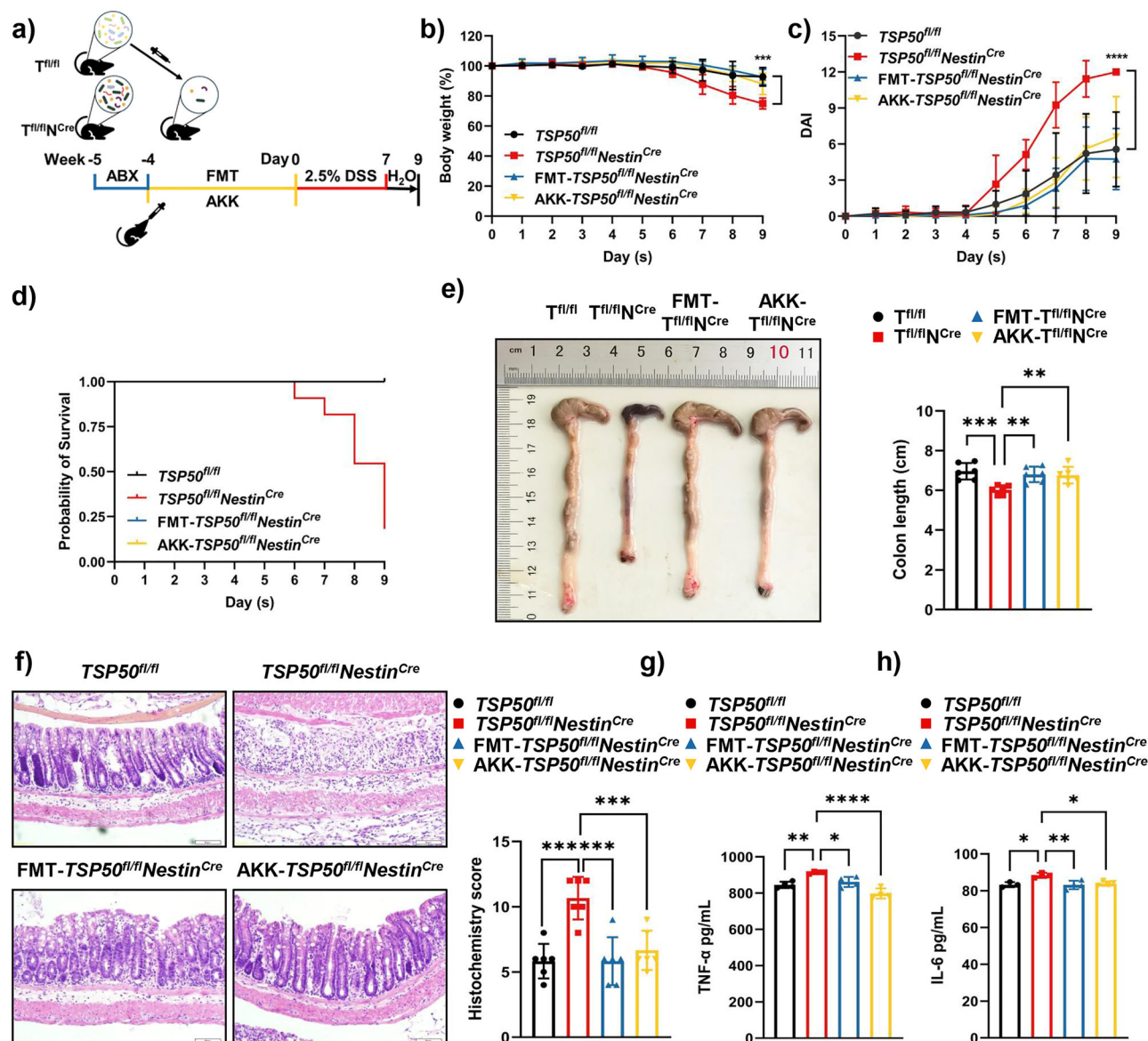
Fig. 4 | FMT and AKK replantation rescues the phenotype of exacerbated colitis caused by TSP50 deficiency in NSCs. a Scheme of FMT and AKK replantation protocol. **b** Body weight loss after DSS treatment ($n = 6$). **c, d** The DAI scores and survival rates after DSS treatment ($n = 6$). **e** Colon lengths and quantification after DSS treatment ($n = 6$). **f** Representative HE staining and histopathological scores of colon tissues after DSS treatment ($n = 6$). Scale bar: 50 μm. **g** ELISA analysis of serum TNF-α levels after DSS treatment ($n = 4$). **h** ELISA analysis of serum IL-6 levels after DSS treatment ($TSP50^{fl/fl}$, $n = 3$; $TSP50^{fl/fl}Nestin^{Cre}$, $n = 3$; FMT-$TSP50^{fl/fl}Nestin^{Cre}$, $n = 4$; AKK-$TSP50^{fl/fl}Nestin^{Cre}$, $n = 4$). Values were expressed as means ± SEM. Two-way ANOVA was used to analyze (**b, c**), one-way ANOVA was used to analyze (**e, f, g, h**). ns (no significance), * $P < 0.05$, ** $P < 0.01$, *** $P < 0.001$, **** $P < 0.0001$.

expression was significantly higher during the remission phase compared to the active phase. Conversely, AChE protein expression was significantly higher in the active stage than in the remission stage (Fig. 7g), suggesting that TSP50 may play different roles in different stages of IBD. Moreover, correlation analysis showed that TSP50 protein expression was negatively correlated with AChE protein expression in both active and remission CD patients (Fig. 7h).

AChE inhibitor neostigmine methyl sulfate (NMS) treatment rescues intestinal mucosal barrier disruption and reduces susceptibility to colitis in *TSP50^{fl/fl}Nestin^{Cre}* mice

To verify the above mechanism, mice were intraperitoneally injected with 20 μg/kg AChE inhibitor NMS. ELISA results showed that intestinal ACh levels were significantly increased in *TSP50^{fl/fl}Nestin^{Cre}* mice treated with NMS, and there was no difference compared with control mice

(Supplementary Fig. 9a). Consistent with this, NMS treatment significantly increased goblet cell numbers and MUC2 secretion in *TSP50^{fl/fl}Nestin^{Cre}* mice, while decreasing intestinal mucosal barrier permeability and alleviating intestinal inflammation (Supplementary Fig. 9b–g), indicating that NMS treatment could restore intestinal mucosal barrier damage in *TSP50^{fl/fl}Nestin^{Cre}* mice.

It has been shown that the administration of AChE inhibitors such as neostigmine and galantamine can alleviate colitis in mice[30,31]. To further explore the role of AChE inhibitor in colitis in *TSP50^{fl/fl}Nestin^{Cre}* mice, DSS was administered to mice during NMS treatment to induce colitis, as shown in Fig. 8a. The results of various indicators for colitis, including weight loss, DAI scores, survival rates, colon length, histological scores, and serum pro-inflammatory cytokine levels, consistently indicated that NMS treatment reduced the susceptibility of *TSP50^{fl/fl}Nestin^{Cre}* mice to colitis (Fig. 8b–h).
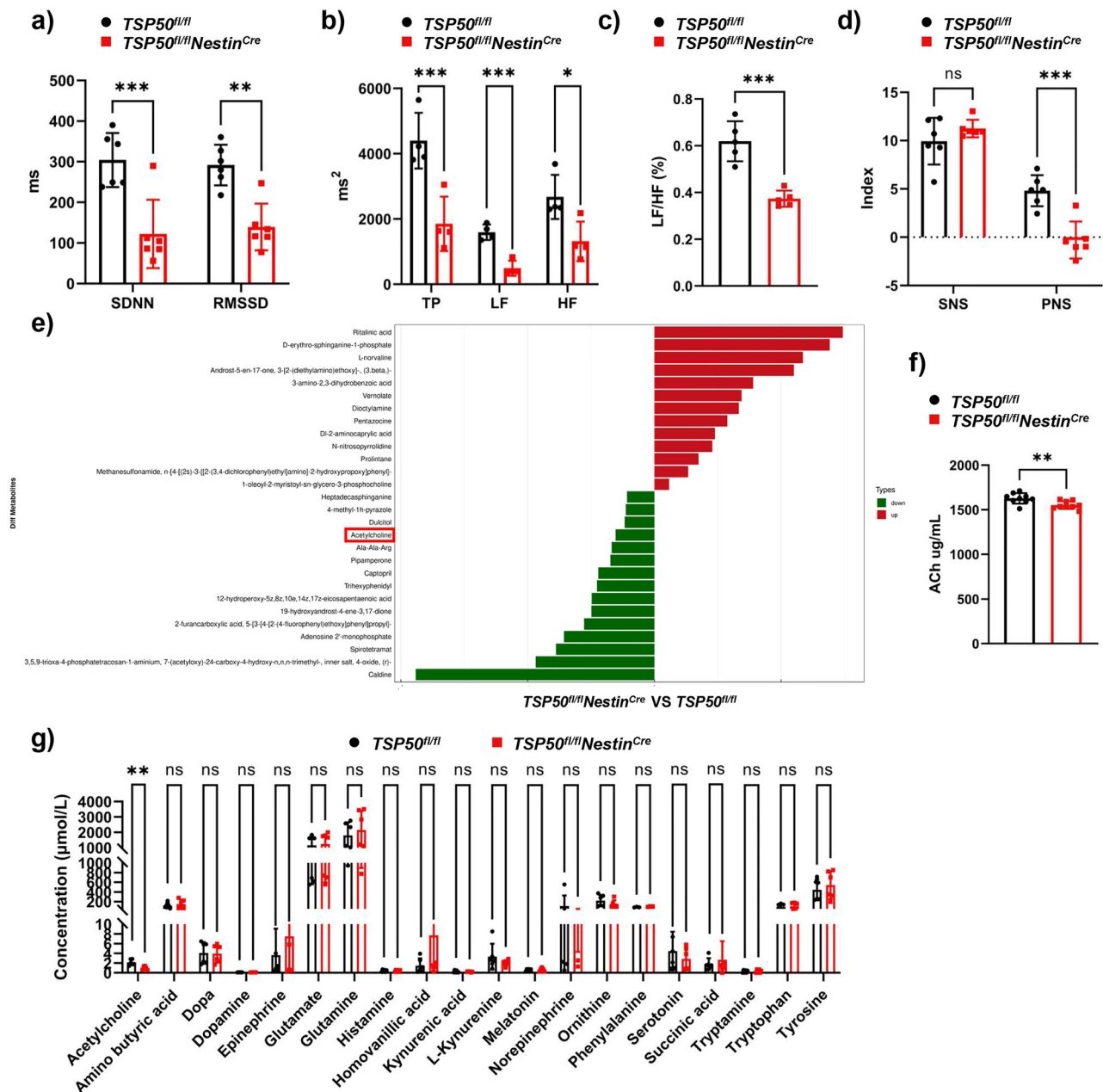
Fig. 5 | TSP50 deficiency in NSCs results in ANS disorders and reduced ACh levels. a Time domain analysis of heart rate variability ($n = 6$). (SDNN: Standard Deviation of Normal-to-Normal Intervals; RMSSD: Root Mean Square of Successive Differences.) b Frequency domain analysis of heart rate variability ($n = 6$). (TP total power, LF low frequency, HF high frequency.) c Ratio of low and high frequency power in heart rate variability ($n = 6$). d SNS and PNS indices in heart rate variability ($n = 6$). e Untargeted metabolic analysis of mice hippocampus. f ELISA analysis of ACh levels in the hippocampus ($n = 9$). g LC-MS analysis of colonic neurotransmitters ($n = 5$). Values were expressed as means ± SEM. One-way ANOVA was used to analyze (a, b, d, g), unpaired two-tailed Student's t test was used to analyze (c, f). ns (no significance), * $P < 0.05$, ** $P < 0.01$, *** $P < 0.001$, **** $P < 0.0001$.

CNS-targeted TSP50 replenishment restores ACh levels and intestinal mucosal barrier integrity, and reduces susceptibility to colitis in *TSP50fl/flNestinCre* mice

Previous studies have shown that intestine-derived TSP50 has an important role in regulating the intestinal mucosal barrier[22]. To further distinguish between the functions of NSCs-derived and intestine-derived TSP50, we conducted experiments using AAV-PHP.eB vectors targeting the CNS to replenish TSP50 in NSCs-TSP50 deficient mice. After intravenously injecting NSCs-TSP50 deficient mice with AAV-PHP.eB vectors overexpressing TSP50 for 6 weeks, we detected TSP50 expression in both the brain and colon. The results revealed that TSP50 expression in the brain of NSCs-TSP50 deficient mice was restored to normal levels, while

TSP50 expression in the intestine remained significantly reduced (Supplementary Fig. 10a). More importantly, replenishing TSP50 specifically in the CNS was found to restore ACh levels, goblet cell numbers, mucin secretion, intestinal mucosal permeability, and intestinal inflammation in NSCs-TSP50 deficient mice (Supplementary Fig. 10b–g). Additionally, the colitis susceptibility of NSCs-TSP50 deficient mice was significantly reduced following this treatment (Supplementary Fig. 11). These experimental results suggest that when only TSP50 in NSCs is replenished, the intestinal mucosal barrier function and colitis susceptibility of NSCs-TSP50 deficient mice return to normal, indicating that the phenotypes observed in our study can primarily be attributed to the function of TSP50 in NSCs.
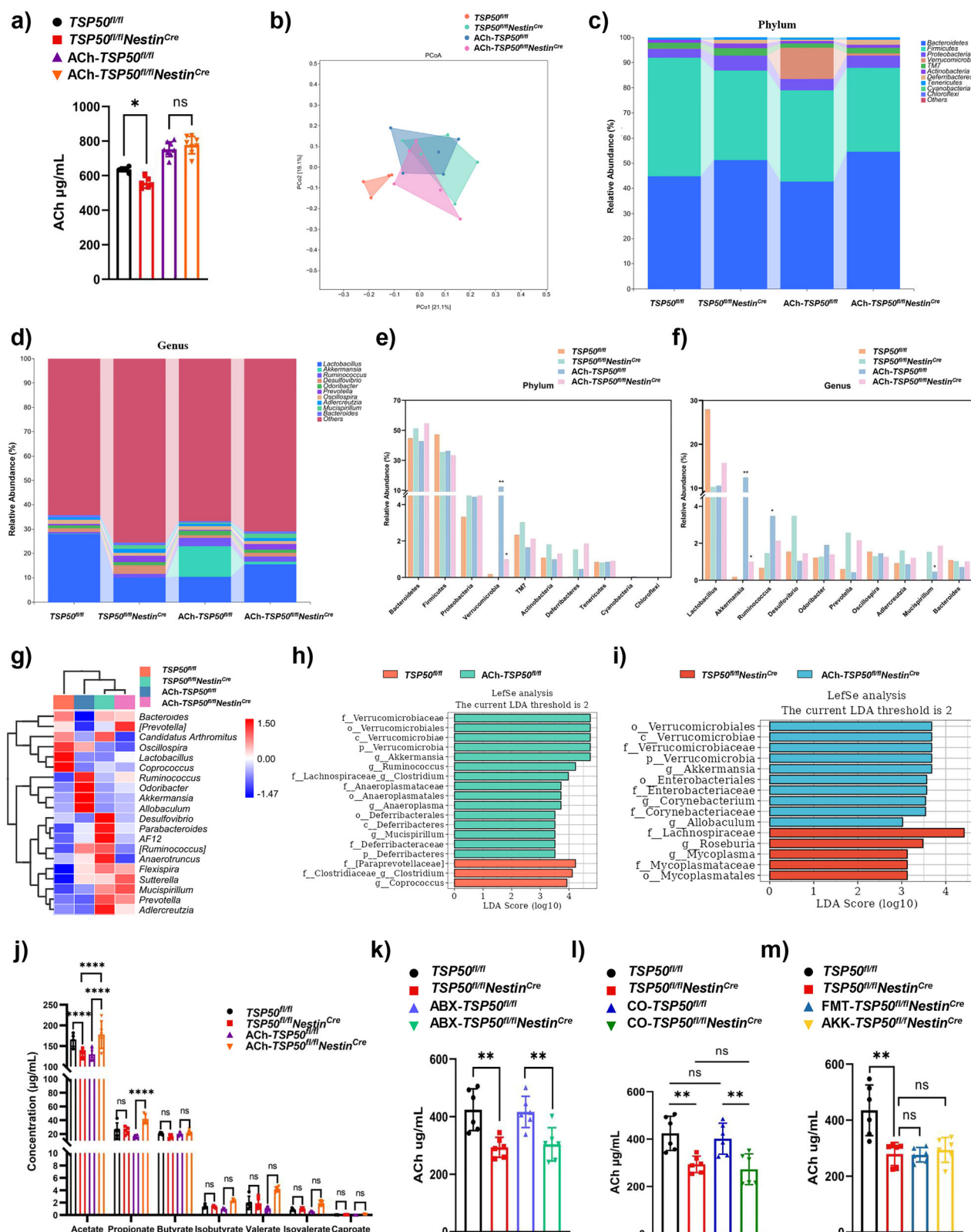
Discussion

Although the exact etiology of IBD is not fully understood, genetic susceptibility is considered as a key factor contributing to its pathogenesis[32]. To date, genome-wide association studies have identified more than 200 IBD risk loci, but they account for only a small fraction of disease susceptibility[33,34]. It is critical to explore potential new candidate risk genes

for IBD and uncover the complex interactions that drive the disease. Recent studies have indicated that most of the genetic risk variants associated with IBD affect the structure of the gut microbiota, and an unbalanced gut microbiota can further activate the immune system and induce intestinal inflammation in genetically susceptible individuals[32,35,36]. TSP50 is a newly identified potential IBD genetic risk factor, but whether it affects colitis

Fig. 6 | ACh supplementation restores the composition of gut microbiota and SCFAs production. a ELISA analysis of ACh levels in the colon after ACh supplementation (*TSP50^fl/fl*, n = 6; *TSP50^fl/fl Nestin^Cre*, n = 6; ACh-*TSP50^fl/fl*, n = 8; ACh-*TSP50^fl/fl Nestin^Cre*, n = 8). **b** PCoA analysis of fecal microbiota using weighted Uni-Frac distances of beta diversity after ACh supplementation. **c** Histogram of phylum-level species composition after ACh supplementation. **d** Histogram of genus-level species composition after ACh supplementation. **e** Histogram of species difference comparison for the top 10 abundances at phylum-level (n = 6). **f** Histogram of species difference comparison for the top 10 abundances at genus-level (n = 6). **g** Heat map of the relative abundance of the dominant genus. **h** LEfSe analysis of differential microbiota in *TSP50^fl/fl* mice before and after ACh treatment. **i** LEfSe analysis of differential microbiota in *TSP50^fl/fl Nestin^Cre* mice before and after ACh treatment. **j** GC-MS analysis of fecal SCFAs after ACh supplementation (n = 5). **k** ELISA analysis of ACh levels in the colon after ABX treatment (n = 6). **l** ELISA analysis of ACh levels in the colon after co-housing treatment (n = 6). **m** ELISA analysis of ACh levels in the colon after FMT and AKK replantation (n = 6). Values were expressed as means ± SEM. One-way ANOVA was used to analyze (**a, j, k, l, m**), Kruskal-Wallis *H* test was used to analyze (**e, f**). ns (no significance), * $P < 0.05$, ** $P < 0.01$, *** $P < 0.001$, **** $P < 0.0001$.

susceptibility through modulation of gut microbiota remains unclear. In this study, we found that TSP50 deficiency in NSCs led to alterations in gut microbiome of mice, particularly a significant reduction in the abundance of *Akkermansia* genus and increased susceptibility to colitis. These findings indicate that host TSP50 gene expression contributes to maintaining the balance between host and microbiota, thus refining the specific mechanisms underlying TSP50 as an IBD risk locus.

In this study, we demonstrated that Nestin-Cre-driven TSP50 knockout resulted in reduced TSP50 levels in both brain and intestinal tissues, which may be attributed to Nestin expression in enteric neural cells[37]. Notably, CNS-targeted TSP50 rescue mediated by AAV-PHP.eB vectors delivery restored intestinal ACh levels in NSCs-specific TSP50 deficient mice, highlighting the dominant role of TSP50 derived from brain NSCs in intestinal ACh regulation. Mechanistically, TSP50-mediated regulation of AChE can control ACh degradation. However, the potential direct effects of TSP50 on neural circuits or ACh secretion, independent of degradation, warrant further exploration.

ACh plays a crucial role in various physiological processes, including gut motility, secretion, and immune regulation and its role in IBD has attracted much attention[38,39]. Our study revealed that TSP50 deficiency in NSCs resulted in reduced colonic ACh levels, decreased goblet cell numbers, and reduced mucin secretion, thereby increasing colitis susceptibility in mice. Importantly, the regulation of goblet cell function and stimulation of mucin secretion by ACh have been well studied[40,41]. For example, ACh enhances mucin secretion by activating the M3 receptors on goblet cells, a process essential for maintaining intestinal mucosal barrier function[42]. This is consistent with our experimental results showing that ACh treatment restored the mucous layer and reduced colitis susceptibility in NSCs-specific TSP50 deficient mice, suggesting that TSP50 most likely affects the intestinal mucosal barrier mucus layer by regulating ACh levels, which in turn affects colitis susceptibility. Targeting ACh may thus be a potential therapeutic strategy for promoting mucosal healing in IBD.

Notably, we also observed that ACh treatment significantly increased the abundance of *Akkermansia* genus in NSCs-specific TSP50 deficient mice. Surprisingly, the gut microbiota of control mice treated with ACh exhibited more pronounced changes, with significant increases in the abundance of *Akkermansia* genus and *Ruminococcus* genus and a significant decrease in the abundance of *Mucispirillum* genus. *Mucispirillum* genus is also a bacteria capable of degrading mucus[43], and its decreased abundance may be intended to partly balance the increased abundance of *Akkermansia* genus. It has been shown that the mucus layer can regulate the growth of commensal and pathogenic microbial communities[44,45]. Therefore, these significant changes in gut microbiota are likely related to the increased mucin secretion stimulated by ACh treatment, especially considering that *Akkermansia* genus is a mucin-dependent bacteria. Combined with our findings that alteration of gut microbiota could not restore colonic ACh levels and mucous layer in NSCs-specific TSP50 deficient mice, we established a positive regulatory relationship: TSP50 regulates ACh, ACh regulates mucous layer, and mucous layer regulates gut microbiota. However, considering the critical role of ACh in immune regulation[46] and the close relationship between immune system and gut microbiota[47], we cannot rule out the possibility that ACh may also affect gut microbiota through immune regulation or other pathways. Further studies are needed to explore these potential mechanisms.

AKK, as a new generation of probiotics, has shown great potential in the treatment of diseases such as IBD[48,49]. Numerous studies have reported an inverse association between AKK and IBD[50–52], and AKK treatment ameliorated colitis and blunted colitis-related tumorigenesis[53–55]. The possible mechanism of AKK in the treatment of colitis is to increase the production of SCFAs[56]. Consistent with this, we found that TSP50 deficiency in NSCs resulted in less *Akkermansia* genus dominated microenvironment, reduced SCFAs acetate production, and increased susceptibility to colitis. Either direct AKK supplementation or indirect AKK restoration by ACh treatment restored SCFAs production and reduced colitis susceptibility. Therefore, we suggest that SCFAs produced by AKK may mediate, at least in part, the modulating effects of NSCs-specific TSP50 deletion on colitis susceptibility. However, several studies have also shown a controversial role for AKK in mouse IBD models. Specifically, the presence of AKK worsened the symptoms of colitis caused by Salmonella typhimurium infection in mice colonized with a simplified human gut microbiome (SIHUMI) composed of eight bacterial species[57]. Additionally, repeated gavage of AKK resulted in an increase in the severity of colitis in IL10$^{-/-}$ mice[58]. These seemingly contradictory results could be explained by strain-specific effects or the pathological context[59]. Therefore, further research is needed to elucidate the mechanisms of action and strain specificity of AKK to ensure its therapeutic efficacy in IBD.

In addition, it is noteworthy that the use of small intestinal organoids from *TSP50^fl/fl Nestin^Cre* mice, which exhibited reduced goblet cell numbers and mucin secretion, reflected the colonic phenotypes observed in vivo, suggesting that TSP50 in NSCs impacts intestinal epithelial function. However, further studies using colonic organoids are needed to confirm these findings, as we used small intestinal organoids due to the currently low differentiation efficiency of colonic organoids.

In summary, our study reveals that TSP50 in NSCs can protect mice from DSS-induced colitis by regulating ACh levels and gut microbiota. These findings provide a new perspective on host-commensal microbiota, which may be beneficial for developing potential therapeutic strategies for IBD.

Methods

Human IBD samples

All samples (n = 19) of IBD patients were obtained from Shenzhen Children's Hospital. The patients' detailed information was provided in Supplementary Table 1. This study was approved by the Institutional Review Board of Shenzhen Children's Hospital (No.2022057) and written informed consent was obtained from all participants. All procedures complied with the Declaration of Helsinki.

Mice

TSP50^flox/flox (*TSP50^fl/fl*) mice, generated as previously described[22], were used as controls in all experiments. *Nestin-Cre* mice were purchased from GemPharmatech Co., Ltd (Nanjing, China). *TSP50^fl/fl Nestin^Cre* mice were generated by crossing *TSP50^fl/fl* mice with *Nestin-Cre* mice. All mice were bred on a C57BL/6J background and kept in a specific pathogen-free environment. Mice were injected with 100 mg/kg pentobarbital sodium for euthanasia. All animal protocols were approved by the Animal Advisory Committee of Northeast Normal University (NENU/IACUC, AP20201029).
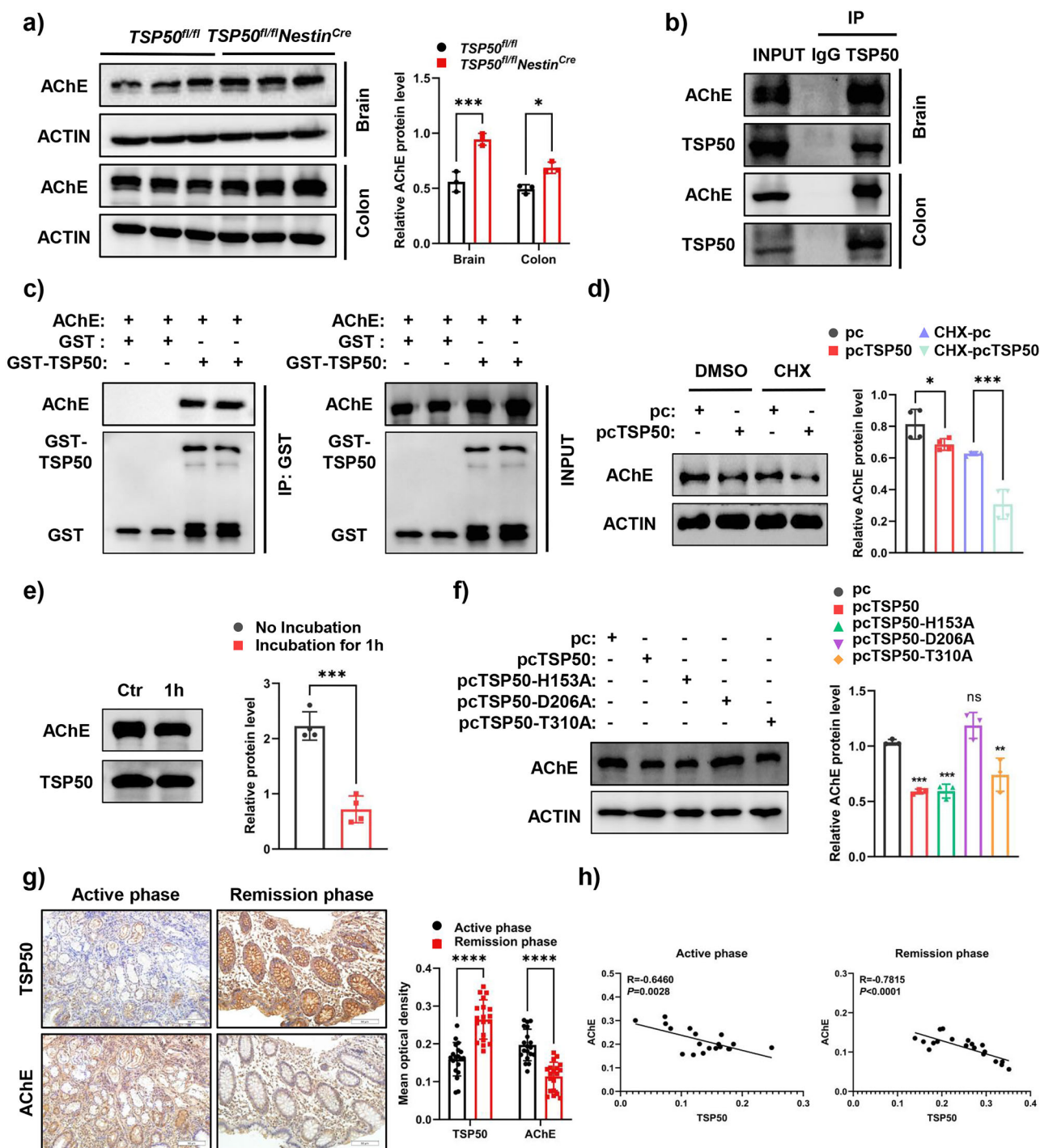
Fig. 7 | TSP50 deficiency in NSCs reduces ACh levels by reducing AChE degradation. a WB analysis and quantification of AChE protein levels in mouse brain and colon ($n = 3$). **b** Co-IP analysis of proteins interacting with TSP50 in mouse brain and colon. **c** GST pull-down of AChE by GST-TSP50 using proteins purified in B21 bacteria, followed by WB analysis. **d** WB analysis and quantification of AChE protein levels in control and TSP50-overexpressing 293T cells after CHX treatment ($n = 4$). **e** WB analysis and quantification of AChE protein levels after incubation with TSP50 protein at 20 mM Tris-HCL (pH7.6) for 1 h at 37 °C ($n = 4$). (Ctr: No incubation; 1 h:

Incubation for 1 h) **f** WB analysis and quantification of TSP50 and AChE protein levels in 293T cells with normal and overexpression TSP50 and different TSP50 mutants ($n = 3$). **g** Representative IHC staining of TSP50 and AChE protein expression in CD patient tissues and quantification ($n = 19$). Scale bar: 50 μm. **h** Pearson correlation analysis was performed between the relative levels of TSP50 and AChE protein in samples of CD patients. Values were expressed as means ± SEM. One-way ANOVA was used to analyze (**a**, **d**, **f**, **g**), unpaired two-tailed Student's *t* test was used to analyze (**e**). ns (no significance), * $P < 0.05$, ** $P < 0.01$, *** $P < 0.001$, **** $P < 0.0001$.

DSS-induced colitis

Mice were treated with 2.5% DSS (TdB, Uppsala, Sweden) in drinking water for 7 days, followed by drinking water for the next 2 days, and then sacrificed. The disease activity index (DAI) was scored daily according to following parameters: weight loss (no loss = 0;

<5% = 1; 5–10% = 2; 10–15% = 3; >15% = 4), stool consistency (normal = 0; soft stool = 1; loose stool = 2; watery stool = 4), and rectal bleeding (no blood = 0; hemocult positive = 1; visual pellet bleeding = 2; gross bleeding or blood around anus = 4). Scores ranged from 0 to 12.
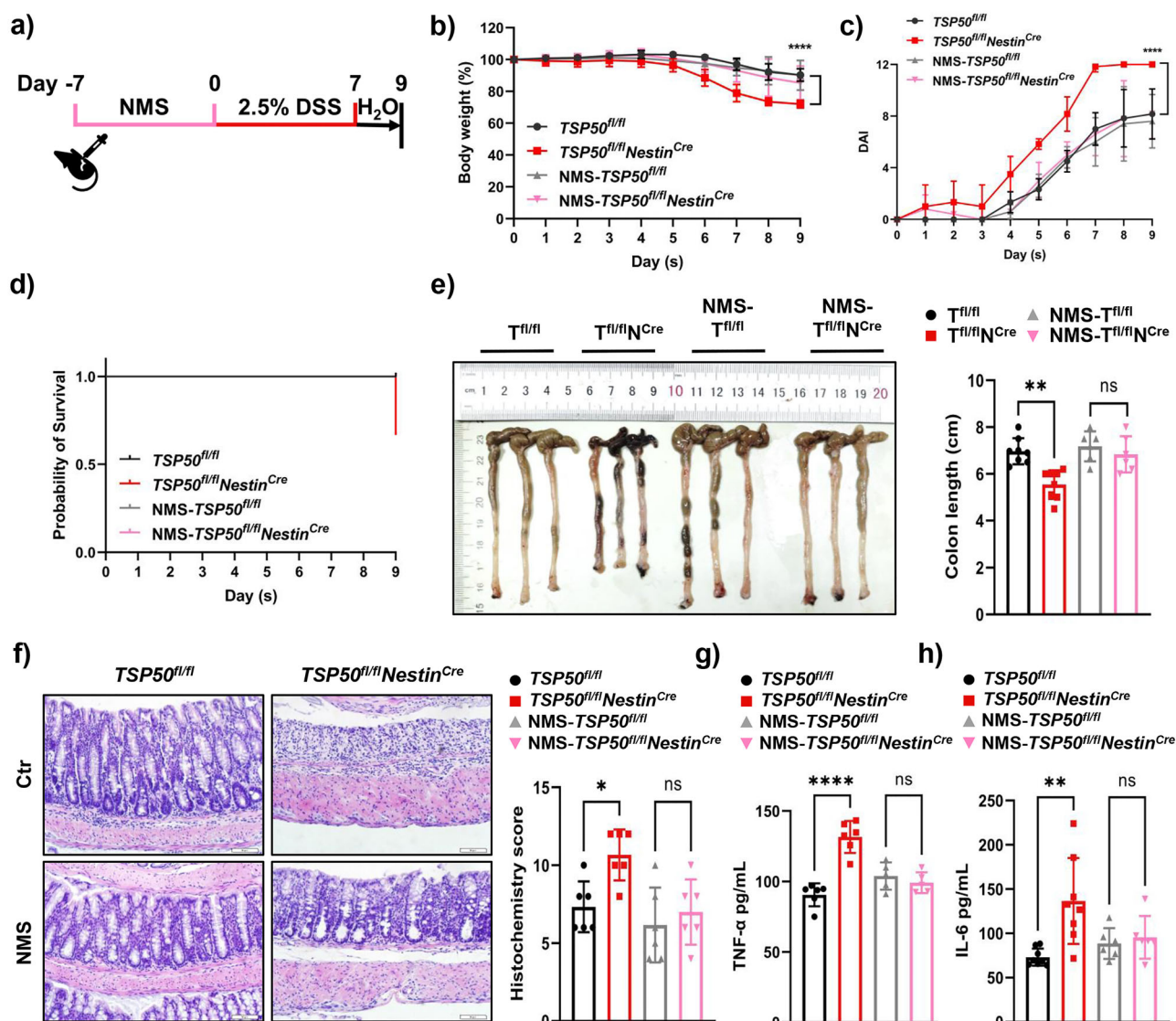
Fig. 8 | AChE inhibitor NMS treatment reduces susceptibility to colitis in *TSP50^{fl/fl} Nestin^{Cre}* mice. a Scheme of NMS treatment protocol. **b** Body weight loss after DSS treatment (*TSP50^{fl/fl}*, n = 8; *TSP50^{fl/fl}Nestin^{Cre}*, n = 8; NMS-*TSP50^{fl/fl}*, n = 6; NMS-*TSP50^{fl/fl}Nestin^{Cre}*, n = 6). **c, d** The DAI scores and survival rates after DSS treatment (*TSP50^{fl/fl}*, n = 8; *TSP50^{fl/fl}Nestin^{Cre}*, n = 8; NMS-*TSP50^{fl/fl}*, n = 6; NMS-*TSP50^{fl/fl} Nestin^{Cre}*, n = 6). **e** Colon lengths and quantification after DSS treatment (*TSP50^{fl/fl}*, n = 8; *TSP50^{fl/fl}Nestin^{Cre}*, n = 8; NMS-*TSP50^{fl/fl}*, n = 6; NMS-*TSP50^{fl/fl}Nestin^{Cre}*, n = 6). (T^{fl/fl}: *TSP50^{fl/fl}*; T^{fl/fl}N^{Cre}: *TSP50^{fl/fl}Nestin^{Cre}*; NMS-T^{fl/fl}: NMS-*TSP50^{fl/fl}*; NMS-T^{fl/fl}N^{Cre}: NMS-*TSP50^{fl/fl}Nestin^{Cre}*). **f** Representative HE staining and histopathological scores of colon tissues after DSS treatment (n = 6). Scale bar: 50 μm. **g** ELISA analysis of serum TNF-α levels after DSS treatment (*TSP50^{fl/fl}*, n = 6; *TSP50^{fl/fl}Nestin^{Cre}*, n = 6; NMS-*TSP50^{fl/fl}*, n = 5; NMS-*TSP50^{fl/fl}Nestin^{Cre}*, n = 5). **h** ELISA analysis of serum IL-6 levels after DSS treatment (*TSP50^{fl/fl}*, n = 8; *TSP50^{fl/fl}Nestin^{Cre}*, n = 8; NMS-*TSP50^{fl/fl}*, n = 6; NMS-*TSP50^{fl/fl}Nestin^{Cre}*, n = 6). Values were expressed as means ± SEM. Two-way ANOVA was used to analyze (**b, c**), one-way ANOVA was used to analyze (**e, f, g, h**). ns (no significance), * $P < 0.05$, ** $P < 0.01$, *** $P < 0.001$, **** $P < 0.0001$.

Histological staining

Mouse colon tissues were collected, fixed in 10% formalin solution, dehydrated by gradient alcohol, embedded in paraffin, and samples were cut into 5 μm paraffin sections. The paraffin sections were then subjected to hematoxylin and eosin (HE) or alcian blue (Solarbio, Beijing, China) staining according to the manufacturer's instructions. IHC and IF staining were performed as previously reported[22]. The sections were incubated with primary antibody: anti-MUC2 (1:1000; ab272692, Abcam, Cambridge, United Kingdom), anti-TSP50 (1:500; 12574-1-AP, Proteintech, Wuhan, China), anti-AChE (1:20; ab2803, Abcam), anti-NESTIN (1:200; 19483-1-AP, Proteintech) and corresponding secondary antibody. Images were acquired via a Nikon Eclipse microscope (Nikon, Tokyo, Japan) or a laser scanning confocal microscope (Zeiss, Oberkochen, Germany).

Histological scoring

Histologic scoring of the colon was assessed based on HE staining observations of colon tissue sections, including crypt architecture, epithelial cell morphology, inflammatory cell infiltration, and glandular morphology. The scoring criteria were as follows: 0 indicating normal, 1 indicating mild abnormality, 2 indicating moderate abnormality, and 3 indicating severe abnormality. Scores ranged from 0 to 12.

RNA extraction and RT-qPCR

Total RNA was isolated using Trizol reagent and cDNAs were synthesized by a RT-PCR Kit (TransGen Biotech, Beijing, China) and specific primers were designed for RT-qPCR detection. The specific primer sequences were shown in Supplementary Table 2. The detection conditions and procedures

were set according to instructions provided in SYBR Green Kit (TransGen Biotech).

Western blot (WB)

The proteins were extracted using RIPA buffer, subsequently separated via SDS–PAGE, and transferred onto a PVDF membrane. After blocking with 5% skim milk, the membranes were incubated with specific primary antibody overnight at 4 °C: anti- TSP50 (1:1000; ab181993, Abcam), anti- AChE (1:1000; ab183591, Abcam), anti- E-CADHERIN (1:1000; 20874-1-AP, Proteintech), anti- OCCLUDIN (1:1000; 27260-1-AP, Proteintech), anti-CLAUDIN-1 (1:1000; 28674-1-AP, Proteintech), followed by incubation of corresponding secondary antibodies (Proteintech, China). The immunoblots were visualized via enhanced chemiluminescence (ECL) solution (Beyotime, Beijing, China).

Co-immunoprecipitation (Co-IP)

The protein was extracted with IP lysis solution and incubated with anti-TSP50 (1:100; ab181993, Abcam) overnight at 4 °C. The next day, sugar beads were added and co-incubated for 4–6 h. The supernatant was removed by centrifugation, and an appropriate amount of 1× loading buffer was added for Western blot assay.

GST pull-down

The GST-TSP50 protein was prepared and purified as described previously[60]. Meanwhile, the pCMV-AChE plasmid was transfected into 293T cells, and the protein was extracted. Then, GST-TSP50 was incubated with GST beads for 3 h. Next, the proteins mentioned above were added to the mixture and mixed for 3 h on a mixer with rotation. Finally, the unbound proteins were discarded and an appropriate amount of 1× loading buffer was added for Western blot assay.

Crypt isolation and organoid culture

After the small intestine was removed and cut into small pieces, it was rinsed thoroughly with DPBS. And then digested with 20 mM EDTA for 40 min, filtered through a 70 μm cell strainer, and crypts were collected, counted, and seeded into matrigel at various densities, and then dropped into the center of a 24-well plate, with 500 μL organoid medium added to each well and medium was changed every 2–4 days. Organoid formation could be observed during 5–7 days. All organoids used in this study were derived from primary cultures of mouse intestinal tissues and were not passaged.

Bacterial translocation assay

Tissue samples from mesentery, liver, spleen and kidney were collected for bacterial culture by using aseptic techniques. The tissue samples were weighed and then homogenized with saline at a ratio of 1:9. After standing, 100 μL of the homogenate supernatant was taken and incubated on Luria-Bertani (LB) agar at 37 °C for 24 h. Any growth of bacteria on the plates was considered as positive.

ABX treatment

During antibiotic feeding, mice were given free access to water containing a cocktail of antibiotics (1 g/L ampicillin, 1 g/L metronidazole, 1 g/L neomycin and 0.5 g/L vancomycin, all from Solarbio) for 4 weeks.

Cohousing experiment

For the cohousing experiment, one *TSP50*^*fl/fl*^ mouse and one *TSP50*^*fl/fl*^*Nestin*^*Cre*^ mouse were housed in one cage at 4 weeks and cohoused for 4–6 weeks.

FMT and AKK supplementation

To better colonize the gut microbiota, recipient mice were treated with a 7-day ABX to deplete the gut microbiota prior to FMT. The fresh feces from *TSP50*^*fl/fl*^ mice were collected and then resuspended in PBS. The 50 mg/mL suspension was mixed vigorously for 3 min, naturally precipitated for 5 min,

and then 200 μL of the supernatant was taken and administered to recipient mice by gavage for 4 weeks. AKK supplemented mice were gavaged with 10^8 CFU/0.2 mL AKK for 4 weeks.

16S rRNA sequencing

Fecal microbiota DNA was extracted using MagPure Stool DNA KF Kit B (Magen Biotechnology Co., Ltd, Beijing, China) and amplified by PCR. The PCR amplification products were purified by Agencourt AMPure XP magnetic beads and dissolved in elution buffer. The fragment range and concentration of the library were examined using an Agilent 2100 Bioanalyzer. The qualified libraries were selected for sequencing by HiSeq platform according to the insert size. After data filtering, the remaining high-quality clean data were used for later analysis. The overlap relationship between reads was used to concatenate reads into tags. Tags were clustered into OTU and compared with Greengene database for species annotation. Based on OTU and annotation results, species complexity analysis of samples, species difference analysis between groups, and association analysis were performed. The protocols were conducted by BGI (Wuhan, China).

Heart rate variability (HRV)

Mice were anesthetized with 0.25% tribromoethanol by intraperitoneal injection, fixed in the supine position, and needle-like electrodes were inserted into the right forelimb and both hind limbs of the mice. LabChart software was used to record the signal for 10–15 min, paying attention to avoid the interference of sound and radio waves at this time. Kubios software was used to analyze the data of the stable part of the collected signal (5 min), including time domain analysis and frequency domain analysis.

Cytokine assay

Cytokine levels in Fig. 1g, h were measured using a fluorescence-based multiplex ELISA microarray system (QAM-INT-1, RayBiotech, GA, USA). Briefly, samples were processed according to the manufacturer's protocol, and signals were acquired using a laser scanner (Cy3 channel). Data were analyzed using the QAM-INT-1 software to calculate cytokine concentrations. For subsequent experiments (Figs. 4g, h and 8g, h), cytokine levels were quantified using conventional single-analyte ELISA kits (Mouse TNF-α ELISA Kit, CB10851-Mu; Mouse IL-6 ELISA Kit, CB10187-Mu; CoBio, Shanghai, China). Absorbance at 450 nm was measured with a microplate reader, and sample concentrations were determined via standard curves generated for each assay. Differences in cytokine level ranges between experiments are attributable to variations in assay methods.

Neurotransmitters assay

Neurotransmitter levels were measured using a combined protocol of metabolite extraction, liquid chromatography, and mass spectrometry (LC-MS/MS). Briefly, tissue samples stored at −80 °C were homogenized in liquid nitrogen, and 60 mg aliquots were processed with 100 μL of 1% formic acid (FA) in ultrapure water. After homogenization, 400 μL of prechilled 1% FA-acetonitrile (ACN) was added, followed by vortexing (30 s), sonication in an ice bath (30 min), and incubation at −20 °C for 1 h. The supernatant was collected after centrifugation (14,000 rcf, 20 min, 4 °C), vacuum-dried, and stored at −80 °C. Dried extracts were reconstituted in 100 μL of 1% FA-ACN/H_2O (1:1, v/v), vortexed, and centrifuged (14,000 rcf, 15 min, 4 °C) before LC-MS/MS analysis. Chromatographic separation was performed using an Agilent 1290 Infinity LC system with a 4 °C autosampler and a 40 °C column. The mobile phases consisted of (A) 50 mM ammonium formate +0.425% FA and (B) methanol, delivered at 400 μL/min with a 2 μL injection volume. The gradient program was: 5–70% B (0–5 min), 70–100% B (5–11 min), 100% B (11–13 min), 100–10% B (13–13.1 min), and 10% B (13.1–16 min). Mass spectrometry was conducted using a 5500 QTRAP instrument in negative ion mode with the following parameters: ion source temperature 450 °C, Gas1/Gas2 45 psi, curtain gas 30 psi, and ion spray voltage 4500 V. Targeted quantification was

achieved using multiple reaction monitoring (MRM). Data were processed using Multiquant 3.0.2 software, and analyte concentrations were determined via external calibration curves. This protocol was executed by Sangon Biotech (Shanghai, China).

SCFAs assay

Fecal SCFAs concentrations were quantified using gas chromatography-mass spectrometry (GC-MS) as follows. For metabolite extraction, thawed fecal samples (4 °C) were homogenized with 20% phosphoric acid (50 μL per 100 mg sample) and 4-methylvaleric acid (internal standard, final concentration: 500 μM), followed by vortex mixing and centrifugation $(14,000 \times g, 20 \text{ min}, 4 °C)$. The supernatant was collected for analysis. GC-MS separation was performed on an Agilent DB-FFAP capillary column with helium carrier gas (1.0 mL/min). The oven temperature program was 90 °C initial, ramped at 10 °C/min to 160 °C, then at 40 °C/min to 240 °C (held for 5 min). A split injection mode (split ratio 10:1, 1 μL injection volume) was applied. Detection utilized a 5977B MSD spectrometer with electron impact ionization (70 eV). Temperatures were set as follows: inlet 250 °C, ion source 230 °C, transfer line 250 °C, and quadrupole 150 °C. Data acquisition operated in SCAN/SIM mode. Chromatographic peaks were integrated using MSD ChemStation software. SCFAs concentrations were calculated against a standard curve. This protocol was conducted by Personalbio (Nanjing, China).

ACh and NMS treatment

For ACh treatment, mice were divided into two groups. One group received intrarectal administration of either 50 μL of H_2O or 25 mg/kg ACh (dissolved in water; Sigma, Missouri, USA) every day for 14 consecutive days to investigate the effects of ACh on healthy mice. The other group was treated with 2.5% DSS to induce colitis starting on day 7 of ACh treatment and administered continuously throughout the 7-day DSS treatment period to assess the effects of ACh on colitis mice.

For NMS treatment, mice were similarly divided into two groups. One group received intraperitoneal injections of 20 μg/kg NMS (Sigma) daily for 14 consecutive days to observe the effects of NMS on healthy mice. The other group was subjected to colitis induction with 2.5% DSS starting on day 7 of NMS treatment, with NMS administration continuing throughout the 7-day DSS treatment period to evaluate the effects of NMS on colitis mice.

AAV-PHP.eB vectors delivery

Empty AAV-PHP.eB vectors and TSP50-overexpressing AAV-PHP.eB vectors were constructed by Vigene Biosciences (Shandong, China). The empty and TSP50-overexpressing AAV-PHP.eB vectors were injected into mice via the tail vein at a dose of 5×10^{13} genome copies per mouse.

Statistical analysis

GraphPad Prism 9 software and IBM SPSS 26 software were used for statistical analysis. All data from at least three independent replicates were presented as mean ± SEM. The data were analyzed using unpaired two-tailed Student's t test, chi-square test, one-way ANOVA, two-way ANOVA, Mann-Whitney U-test or Kruskal-Wallis H test analysis. Pearson correlation analysis was used to analyze the correlation. Statistical significance was indicated as follows: ns (no significance), $*P < 0.05$, $**P < 0.01$, $***P < 0.001$, $****P < 0.0001$.

Data availability

Sequence data that support the findings of this study have been deposited in the National Center for Biotechnology Information (NCBI) Sequence Read Archive (SRA) database (https://www.ncbi.nlm.nih.gov/sra) with the accession numbers PRJNA1158198 and PRJNA1158006.

References

1. Kaplan, G. G. & Windsor, J. W. The four epidemiological stages in the global evolution of inflammatory bowel disease. *Nat. Rev. Gastroenterol. Hepatol.* **18**, 56–66 (2021).
2. Wang, R., Li, Z., Liu, S. & Zhang, D. Global, regional and national burden of inflammatory bowel disease in 204 countries and territories from 1990 to 2019: a systematic analysis based on the Global Burden of Disease Study 2019. *BMJ Open* **13**, e065186 (2023).
3. Villablanca, E. J., Selin, K. & Hedin, C. R. H. Mechanisms of mucosal healing: treating inflammatory bowel disease without immunosuppression?. *Nat. Rev. Gastroenterol. Hepatol.* **19**, 493–507 (2022).
4. Cai, Z., Wang, S. & Li, J. Treatment of inflammatory bowel disease: a comprehensive review. *Front. Med.* **8**, 765474 (2021).
5. Lu, Y. et al. Gut microbiota influence immunotherapy responses: mechanisms and therapeutic strategies. *J. Hematol. Oncol.* **15**, 47 (2022).
6. Afzaal, M. et al. Human gut microbiota in health and disease: unveiling the relationship. *Front. Microbiol.* **13**, 999001 (2022).
7. Akhtar, M. et al. Gut microbiota-derived short chain fatty acids are potential mediators in gut inflammation. *Anim. Nutr.* **8**, 350–360 (2022).
8. Haneishi, Y. et al. Inflammatory bowel diseases and gut microbiota. *Int. J. Mol. Sci.* **24**, https://doi.org/10.3390/ijms24043817 (2023).
9. Sharkey, K. A. & Mawe, G. M. The enteric nervous system. *Physiol. Rev.* **103**, 1487–1564 (2023).
10. Gervasi, T. & Mandalari, G. The interplay between gut microbiota and central nervous system. *Curr. Pharm. Des.* **29**, 3274–3281 (2023).
11. Dicks, L. M. T. Gut bacteria and neurotransmitters. *Microorganisms* **10**, https://doi.org/10.3390/microorganisms10091838 (2022).
12. Fung, T. C. et al. Intestinal serotonin and fluoxetine exposure modulate bacterial colonization in the gut. *Nat. Microbiol.* **4**, 2064–2073 (2019).
13. Strandwitz, P. et al. GABA-modulating bacteria of the human gut microbiota. *Nat. Microbiol.* **4**, 396–403 (2019).
14. Chu, H. et al. Gene-microbiota interactions contribute to the pathogenesis of inflammatory bowel disease. *Science* **352**, 1116–1120 (2016).
15. Daniel, N. & Chassaing, B. The hidden effect of Nod2 in the host/microbiota relationship. *Cell. Mol. Gastroenterol. Hepatol.* **10**, 424–425 (2020).
16. Lavoie, S. et al. The Crohn's disease polymorphism, ATG16L1 T300A, alters the gut microbiota and enhances the local Th1/Th17 response. *eLife* **8**, https://doi.org/10.7554/eLife.39982 (2019).
17. Yuan, L. et al. Isolation of a novel gene, TSP50, by a hypomethylated DNA fragment in human breast cancer. *Cancer Res.* **59**, 3215–3221 (1999).
18. Song, Z. B. et al. The catalytic triad of testes-specific protease 50 (TSP50) is essential for its function in cell proliferation. *Cell. Signal.* **26**, 2266–2275 (2014).
19. Niu, C. X. et al. PRSS50-mediated inhibition of MKP3/ERK signaling is crucial for meiotic progression and sperm quality. *Zool. Res.* **45**, 1037–1047 (2024).
20. Ai, H. H. et al. Expression and effects of TSP50 in mouse embryo and cardiac myocyte development. *Biochem. Biophys. Res. Commun.* **502**, 283–288 (2018).
21. Zillich, L. et al. Epigenetic signatures of smoking in five brain regions. *J. Pers. Med.* **12**, https://doi.org/10.3390/jpm12040566 (2022).
22. Li, J. et al. TSP50 attenuates DSS-induced colitis by regulating TGF-β signaling mediated maintenance of intestinal mucosal barrier integrity. *Adv. Sci.* **11**, e2305893 (2024).
23. Beutler, L. R. A CNS circuit that regulates gut motility. *Nat. Metab.* **5**, 1452–1453 (2023).
24. Collins, S. M. & Bercik, P. The relationship between intestinal microbiota and the central nervous system in normal gastrointestinal function and disease. *Gastroenterology* **136**, 2003–2014 (2009).

25. Kong, C. et al. Restore intestinal barrier integrity: an approach for inflammatory bowel disease therapy. *J. Inflamm. Res.* **17**, 5389–5413 (2024).

26. Gustafsson, J. K. & Johansson, M. E. V. The role of goblet cells and mucus in intestinal homeostasis. *Nat. Rev. Gastroenterol. Hepatol.* **19**, 785–803 (2022).

27. Stolfi, C., Maresca, C., Monteleone, G. & Laudisi, F. Implication of intestinal barrier dysfunction in gut dysbiosis and diseases. *Biomedicines* **10**, https://doi.org/10.3390/biomedicines10020289 (2022).

28. Zhang, Z. et al. Regulatory role of short-chain fatty acids in inflammatory bowel disease. *Cell Commun. Signal.* **20**, 64 (2022).

29. Luque, F. J. & Muñoz-Torrero, D. Acetylcholinesterase: a versatile template to coin potent modulators of multiple therapeutic targets. *Acc. Chem. Res.* **57**, 450–467 (2024).

30. Singh, S. P. et al. Acetylcholinesterase inhibitor pyridostigmine bromide attenuates gut pathology and bacterial dysbiosis in a murine model of ulcerative colitis. *Dig. Dis. Sci.* **65**, 141–149 (2020).

31. Wazea, S. A., Wadie, W., Bahgat, A. K. & El-Abhar, H. S. Galantamine anti-colitic effect: role of alpha-7 nicotinic acetylcholine receptor in modulating Jak/STAT3, NF-κB/HMGB1/RAGE and p-AKT/Bcl-2 pathways. *Sci. Rep.* **8**, 5110 (2018).

32. Cohen, L. J., Cho, J. H., Gevers, D. & Chu, H. Genetic factors and the intestinal microbiome guide development of microbe-based therapies for inflammatory bowel diseases. *Gastroenterology* **156**, 2174–2189 (2019).

33. de Lange, K. M. et al. Genome-wide association study implicates immune activation of multiple integrin genes in inflammatory bowel disease. *Nat. Genet.* **49**, 256–261 (2017).

34. Graham, D. B. & Xavier, R. J. Pathway paradigms revealed from the genetics of inflammatory bowel disease. *Nature* **578**, 527–539 (2020).

35. Imhann, F. et al. Interplay of host genetics and gut microbiota underlying the onset and clinical presentation of inflammatory bowel disease. *Gut* **67**, 108–119 (2018).

36. Wang, Y. et al. Ring1a protects against colitis through regulating mucosal immune system and colonic microbial ecology. *Gut microbes* **15**, 2251646 (2023).

37. Belkind-Gerson, J. et al. Nestin-expressing cells in the gut give rise to enteric neurons and glial cells. *Neurogastroenterol. Motil.* **25**, 61–69.e67 (2013).

38. Mogilevski, T., Burgell, R., Aziz, Q. & Gibson, P. R. Review article: the role of the autonomic nervous system in the pathogenesis and therapy of IBD. *Aliment. Pharmacol. Ther.* **50**, 720–737 (2019).

39. Zheng, W. et al. Acetylcholine ameliorates colitis by promoting IL-10 secretion of monocytic myeloid-derived suppressor cells through the nAChR/ERK pathway. *Proc. Natl. Acad. Sci. USA* **118**, https://doi.org/10.1073/pnas.2017762118 (2021).

40. Specian, R. D. & Neutra, M. R. Mechanism of rapid mucus secretion in goblet cells stimulated by acetylcholine. *J. Cell Biol.* **85**, 626–640 (1980).

41. Gustafsson, J. K. et al. An ex vivo method for studying mucus formation, properties, and thickness in human colonic biopsies and mouse small and large intestinal explants. *Am. J. Physiol. Gastrointest. Liver Physiol.* **302**, G430–G438 (2012).

42. Gustafsson, J. K. et al. Intestinal goblet cells sample and deliver lumenal antigens by regulated endocytic uptake and transcytosis. *eLife* **10**, https://doi.org/10.7554/eLife.67292 (2021).

43. Herp, S., Durai Raj, A. C., Salvado Silva, M., Woelfel, S. & Stecher, B. The human symbiont Mucispirillum schaedleri: causality in health and disease. *Med. Microbiol. Immunol.* **210**, 173–179 (2021).

44. Paone, P. & Cani, P. D. Mucus barrier, mucins and gut microbiota: the expected slimy partners?. *Gut* **69**, 2232–2243 (2020).

45. Luis, A. S. & Hansson, G. C. Intestinal mucus and their glycans: a habitat for thriving microbiota. *Cell host microbe* **31**, 1087–1100 (2023).

46. Cox, M. A. et al. Beyond neurotransmission: acetylcholine in immunity and inflammation. *J. Intern. Med.* **287**, 120–133 (2020).

47. Yoo, J. Y., Groer, M., Dutra, S. V. O., Sarkar, A. & McSkimming, D. I. Gut Microbiota and Immune System Interactions. *Microorganisms* **8**, https://doi.org/10.3390/microorganisms8101587 (2020).

48. Rodrigues, V. F. et al. Akkermansia muciniphila and gut immune system: a good friendship that attenuates inflammatory bowel disease, obesity, and diabetes. *Front. Immunol.* **13**, 934695 (2022).

49. Zheng, M. et al. The role of Akkermansia muciniphila in inflammatory bowel disease: current knowledge and perspectives. *Front. Immunol.* **13**, 1089600 (2022).

50. Earley, H. et al. The abundance of Akkermansia muciniphila and its relationship with sulphated colonic mucins in health and ulcerative colitis. *Sci. Rep.* **9**, 15683 (2019).

51. Pittayanon, R. et al. Differences in gut microbiota in patients with vs without inflammatory bowel diseases: a systematic review. *Gastroenterology* **158**, 930–946.e931 (2020).

52. Lo Sasso, G. et al. Inflammatory bowel disease-associated changes in the gut: focus on kazan patients. *Inflamm. Bowel Dis.* **27**, 418–433 (2021).

53. Bian, X. et al. Administration of Akkermansia muciniphila ameliorates dextran sulfate sodium-induced ulcerative colitis in mice. *Front. Microbiol.* **10**, 2259 (2019).

54. Wang, L. et al. A purified membrane protein from Akkermansia muciniphila or the pasteurised bacterium blunts colitis associated tumourigenesis by modulation of CD8(+) T cells in mice. *Gut* **69**, 1988–1997 (2020).

55. Jiang, Y. et al. Acetyltransferase from Akkermansia muciniphila blunts colorectal tumourigenesis by reprogramming tumour microenvironment. *Gut* **72**, 1308–1318 (2023).

56. Zhai, R. et al. Strain-specific anti-inflammatory properties of two akkermansia muciniphila strains on chronic colitis in mice. *Front. Cell. Infect. Microbiol.* **9**, 239 (2019).

57. Ganesh, B. P., Klopfleisch, R., Loh, G. & Blaut, M. Commensal Akkermansia muciniphila exacerbates gut inflammation in Salmonella Typhimurium-infected gnotobiotic mice. *PloS ONE* **8**, e74963 (2013).

58. Seregin, S. S. et al. NLRP6 protects Il10(-/-) mice from colitis by limiting colonization of Akkermansia muciniphila. *Cell Rep.* **19**, 733–745 (2017).

59. Zhang, T., Ji, X., Lu, G. & Zhang, F. The potential of Akkermansia muciniphila in inflammatory bowel disease. *Appl. Microbiol. Biotechnol.* **105**, 5785–5794 (2021).

60. Gao, F. et al. TSP50 promotes the Warburg effect and hepatocyte proliferation via regulating PKM2 acetylation. *Cell Death Dis.* **12**, 517 (2021).

Acknowledgements

Author contributions

X.L. performed experiments, analyzed data and wrote the manuscript. R.J. performed experiments and analyzed data. Z.W., H.Z., X.Q. provided clinical patient samples and ethical proof. C.N. helped with animal experiments and cellular experiments. Z.S. helped write the manuscript. X.L. helped in generation and management of mice. J.H. analyzed the sequencing data. F.G., S.W., C.Y., L.S., Y.H. provided critical comments and suggestions.

Competing interests

The authors declare no competing interests.

Additional information

Supplementary information The online version contains supplementary material available at https://doi.org/10.1038/s41522-025-00737-3.

Correspondence and requests for materials should be addressed to Xiaoguang Yang, Yongli Bao or Jiawei Li.

Reprints and permissions information is available at http://www.nature.com/reprints

Publisher's note Springer Nature remains neutral with regard to jurisdictional claims in published maps and institutional affiliations.